Group-common and individual-specific effects of structure-function coupling in human brain networks with graph neural networks

Peiyu Chen[1,#], Hang Yang[1,#], Xin Zheng[1], Hai Jia[1], Jiachang Hao[1], Xiaoyu Xu[1,2], Runsen Chen[3], Tatsuo S. Okubo[1,*], Zaixu Cui[1,*]

[1]Chinese Institute for Brain Research, Beijing, 102206, China

[2]State Key Laboratory of Cognitive Neuroscience and Learning, Beijing Normal University, Beijing, 100091, China

[3]Vanke School of Public Health, Tsinghua University, Beijing, China

[#]Co-first author

[*]Correspondence: cuizaixu@cibr.ac.cn (Z.C.); tatsuo.okubo@cibr.ac.cn (T.S.O.)

Abstract

The human cerebral cortex is organized into functionally segregated but synchronized regions connected by the structural connectivity of white matter pathways. While the structure-function coupling has been implicated in cognitive development and neuropsychiatric disorders, it remains unclear to what extent the coupling reflects a group-common characteristic or varies across individuals at global and regional levels. Leveraging two independent, high-quality datasets, we found that the graph neural network predicted unseen individuals' functional connectivity from structural connectivity more accurately than previous studies, reflecting a strong structure-function coupling. This coupling was primarily driven by network topology and was substantially stronger than linear models. We also found that structure-function coupling was dominated by the group-common effects, with subtle yet significant individual-specific effects. The regional group and individual effects in the coupling were both hierarchically organized across the cortex along a sensorimotor-association cortical axis, with lower group effects and higher individual effects in association cortices. These findings emphasize the importance of considering the group and individual effects in cortical structure-function coupling, suggesting insights into connectivity-guided therapeutics.

Introduction

The human cerebral cortex is organized into functionally segregated neuronal populations connected by the anatomical pathways. White matter fiber tracts form a connectome of structural connectivity at the macroscale[1]. This structural connectome exhibits a complex network topology characterized by non-random properties, including small-world architecture[2], segregated communities[3], and a core of densely inter-connected hubs[4]. These topological patterns support the communication dynamics on structural networks and coordinate the temporal synchronization of neural activity—termed functional connectivity—between cortical regions[5-8]. Understanding how structural connectivity shapes functional connectivity patterns is central to neuroscience.

Convergent evidence from multiple independent studies indicates a reliable coupling between structural and functional connectivity at both global and regional levels using both non-invasive MRI techniques and invasive recordings[9-24]. The structure-function coupling is heterogeneously distributed across the cerebral cortex, exhibiting higher coupling in the primary sensorimotor cortex and lower coupling in the higher-order association cortex[10-12]. This spatial distribution pattern aligns with the sensorimotor-association cortical hierarchy of cytoarchitectonic structure, functional specialization, and evolutionary expansion[10,11,25]. The structure-function coupling shows a developmental increase in regions of association cortex during adolescence with the most prominent effects localized in the default mode network[10]. In contrast, the highly evolutionarily conserved sensorimotor regions exhibit age-related decreases in structure-function coupling throughout adolescence[10] and the whole lifespan[13]. Moreover, higher structure-function coupling has been related to better performance in executive function[10,22], and abnormal patterns of the coupling are associated with a wide range of psychiatric and neurological disorders, such as major

depressive disorder[26], bipolar disorder[27], attention deficit hyperactivity disorder[28], and Parkinson's disease[29].

While structure-function coupling has been extensively implicated in development, cognition, and clinical outcomes[10,13,22,27,28,30], few studies have explicitly examined the extent to which structure-function coupling reflects a group-common characteristic or varies across individuals. Prior studies have reported that functional connectivity is dominated by stable group and individual factors equally[31], and structural connectivity is even less variable than functional connectivity across participants[32], suggesting the structure-function coupling could mainly reflect group rather than individual characteristics. Using six independent datasets, Zimmermann and colleagues found that the individual-specific effects of structure-function coupling can only be observed in one of six datasets[32]. Such a conflicting result could arise from the application of the linear association, which solely accounts for the coupling of direct structural connectivity and ignores indirect functional communications. Moreover, this prior study only examined global structure-function coupling[32]; how the group and individual effects of regional structure-function coupling are distributed across the cortex remains unclear.

Prior studies typically employed linear associations to account for structure-function coupling of direct structural connectivity only[9,10,29,32], or used interpretable models with explicit assumptions for indirect functional communication[6,11,13,21]. Nevertheless, these studies suffered from limited coupling strength between structural and functional connectivity, raising the possibility that the current set of interpretable models potentially overlooked important higher-order functional communication on structural networks. Recently, Sarwar and colleagues have demonstrated that a

powerful feed-forward fully-connected neural network accurately predicted unseen individual's functional connectivity with structural connectivity (group: r = 0.9, individual: r = 0.55)[15], suggesting a potentially much greater structure-function coupling compared to the interpretable communication models. However, randomizing structural networks' topology only resulted in a 20% to 50% reduction in prediction accuracy[15], suggesting the limited contribution from network topology. In contrast to traditional deep learning methods, the graph neural networks (GNN)[33] can inherently capture the communication between the nodes based on the graph (network) topology and have achieved success in the prediction tasks with a variety kinds of topological data, such as spatial cellular networks[34] and protein-protein networks[35]. Two recent studies employed GNN to predict functional connectivity with structural connectivity, however, they did not explicitly evaluate how the network topology contributed to the prediction[36,37].

Here, we proposed to use graph neural networks to address the magnitude of group and individual effects of the structure-function coupling at both global and regional levels. We aim to test three inter-related hypotheses. First, we hypothesized that the graph neural network would accurately predict functional connectivity from structural networks. We also hypothesized that this prediction would primarily be contributed by higher-order network topology, as graph neural networks inherently operate on this aspect[33]. Second, we hypothesized that structure-function coupling would mainly reflect group-common characteristics; however, there still exists a significant amount of individual effect given the implications of structure-function coupling in human individual differences[10,13]. Third, we hypothesized that both the group and individual effects at the regional level would be distributed across the cortex along the sensorimotor-association axis[25]. Specifically, we expected that the group effects of regional structure-function coupling would be

higher in primary sensorimotor cortex, due to relatively minor inter-individual variability in both structural and functional connectivity[38,39]. Conversely, we expected that the individual-specific effects of the coupling would be higher in the higher-order association cortex, where the functional communication may have become untethered from genetic and anatomical constraints[40].

Results

We utilized two independent datasets, namely the unrelated Human Connectome Project (HCP)-young adult (HCP-YA, n = 245, 114 males, aged 22–35 years)[41] and HCP-development (HCP-D, n = 404, 176 males, aged 8–21 years)[42], to evaluate the structure-function coupling. As illustrated in **Fig. 1a**, we first constructed the connectome of functional connectivity (FC) and structural connectivity (SC) for each participant, using the a priori Schaefer cortical parcellation atlas of 400 regions[43]. Particularly, based on the resting-state fMRI data, FC was defined as the Pearson correlation coefficients between each pair of regional time series, resulting in a 400×400 symmetrical FC matrix for each participant. The matrix consisted of 79,800 unique elements, with each element denoted as an "edge" connecting two cortical regions. Fisher r-to-z was applied to improve the normality of FC edge strength. Meanwhile, using the diffusion MRI data, we reconstructed the whole-brain white matter tracts of individual participants via probabilistic fiber tractography with multi-shell, multi-tissue constrained spherical deconvolution (CSD)[44]. Anatomically constrained tractography (ACT)[45] and spherical deconvolution informed filtering of tractograms (SIFT)[46] were applied to improve the biological accuracy of fiber reconstruction. For each participant, we quantified the number of streamlines connecting every pair of cortical regions from the Schaefer atlas to construct a structural connectome of streamline counts. The edge weights of the SC matrix were log-transformed.

To fully investigate the indirect functional communication and non-linear association between structural and functional connectomes, we used a graph neural network (GNN) framework to capture the structure-function coupling by predicting the empirical FC from SC[36,37]. The GNN framework treats each FC edge as higher-order communication through the SC between the corresponding two nodes. Specifically, our GNN model employed a 2-layer graph convolutional network[47], which takes SC as input and aggregates the 2-hop neighboring SC for each node to construct its node embeddings. Then, a 2-layer multilayer perceptron takes each pair of node embeddings as input to predict their connected FC (**Fig. 1a**). For both HCP-YA and HCP-D datasets, we randomly split the participants into two subsets, with one as the training set and the other as the testing set. We used the model trained from the training set to predict the FC in the testing set. We defined the Pearson correlation between the predicted and empirical FC as the structure-function coupling for each participant in the testing set. The following GNN-based coupling analyses were restricted to the testing set.

We presented the group-averaged connectivity matrices of SC, empirical FC, and predicted FC from GNN in the HCP-YA dataset as examples (**Fig. 1b**). The connectivity matrix was organized based on the large-scale functional network affiliations of the 400 cortical regions to the Yeo 7 networks[48], which consists of the visual, somatomotor, dorsal attention, ventral attention, frontoparietal, limbic, and default mode networks. We observed that the predicted FC matrix was very similar to the empirical FC matrix (**Fig. 1b**), suggesting the effectiveness of our GNN model. See **Fig. S1** for both the empirical and predicted connectivity matrices of the HCP-D dataset.

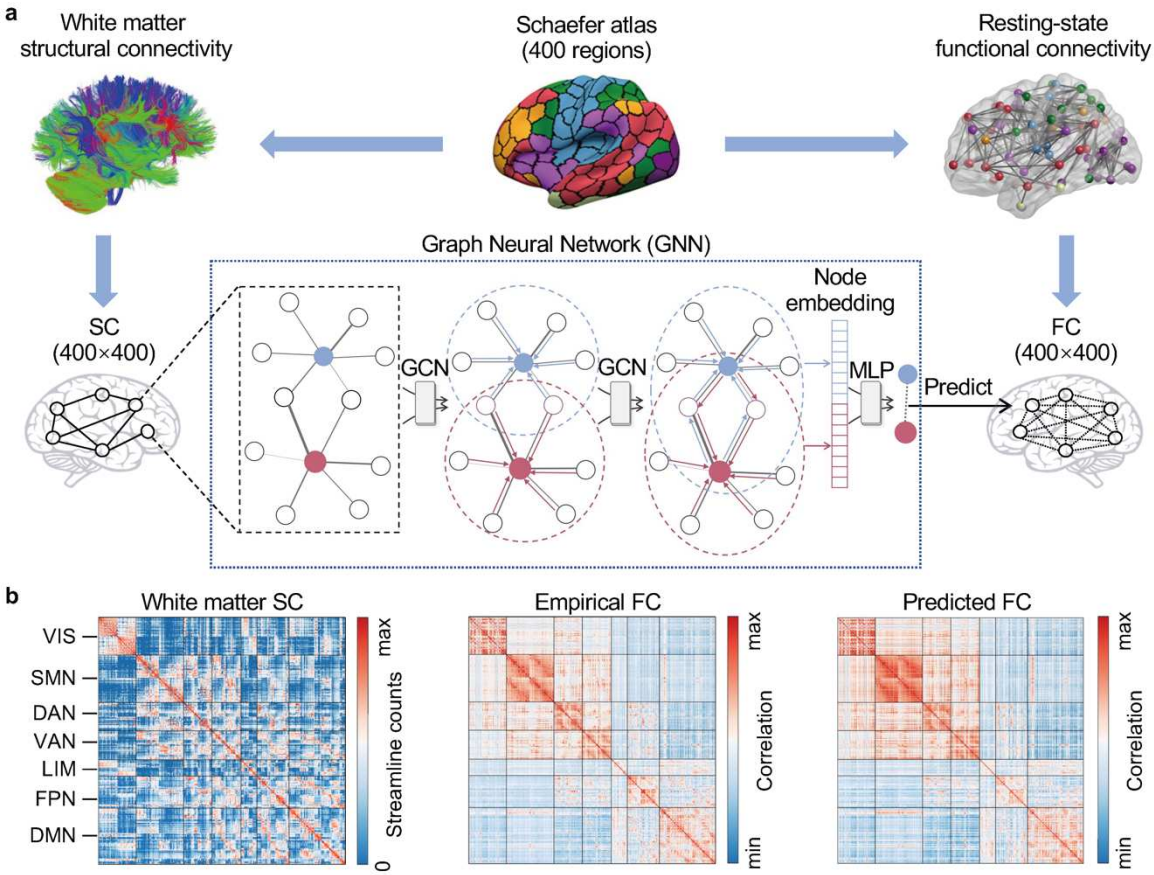

Fig. 1 | The GNN-based framework predicts functional connectivity from structural connectivity. a, For each individual, the white matter structural connectivity (SC) and resting-state functional connectivity (FC) were constructed using the Schaefer-400 atlas. Both structural and functional connectivity can be characterized as a 400×400 matrix, respectively. We applied a graph neural network (GNN) model to predict FC from SC. Specifically, the GNN employs a two-layer graph convolutional network (GCN) to get the node embedding for each node and uses a two-layer multilayer perceptron (MLP) to predict each FC edge from the corresponding two node embeddings. **b**, The group-averaged connectivity matrix of SC, empirical FC, and predicted FC in the HCP-YA dataset. Visual inspection suggests a highly consistent connectional pattern between the empirical and predicted FC matrices. HCP-YA, HCP young adult; VIS, visual network; SMN, somatomotor network; DAN, dorsal attention network; VAN, ventral attention network; LIM, limbic network; FPN, frontoparietal network; DMN, default mode network.

GNN accurately captures the coupling between structural and functional network topology

Prior studies have consistently demonstrated a robust coupling between structural and functional connectivity using a linear association[9-11]. Here, we evaluated if this is true in our dataset. We acquired the group-average empirical FC and SC matrices and flattened the upper triangle elements

into a vector for both matrices. The linear association (i.e., Pearson correlation) demonstrated a positive coupling between FC and SC across all the edges with non-zero SC strength in both HCP-YA ($r = 0.408$, $P < 1\times10^{-16}$; **Fig. 2a**) and HCP-D ($r = 0.429$, $P < 1\times10^{-16}$; **Fig. 2b**) datasets at the group level. These results were consistent with prior reported effect size of group-level structure-function coupling using the linear association[10].

The linear association model only accounts for the direct connections between nodes, while functional connectivity can emerge from polysynaptic communication on structural connectome[5,6]. A recent study indicated that a feed-forward fully-connected neural network accurately predicted FC from SC with a higher accuracy than the coupling with linear association. However, in this work, the network topology had limited contribution to the prediction[49]. We extended these results by applying the GNN model to predict FC with SC, which has the potential to capture more information about the structural network topology[33]. We found that, at the group level, the correlation between the predicted and empirical FCs was $r = 0.942$ ($P < 1\times10^{-16}$; **Fig. 2c**) for HCP-YA and $r = 0.953$ ($P < 1\times10^{-16}$; **Fig. 2d**) for HCP-D dataset. This result suggested that GNN captured a much higher structure-function coupling compared to the linear association at the group level. Moreover, this group-level prediction accuracy was also slightly higher than that from a fully-connected neural network as reported in the prior work (i.e., $r = 0.9$)[15].

We next evaluated whether GNN outperformed traditional approaches at the individual level. Using the linear association, we found that the correlation between FC and SC ranges from Pearson $r = 0.233$ to $r = 0.414$ ($r = 0.315 \pm 0.029$; **Fig. 2e**) across HCP-YA participants and ranges from $r = 0.228$ to $r = 0.427$ ($r = 0.321 \pm 0.027$; **Fig. 2f**) across HCP-D participants. In contrast, GNN

predicted FC from SC with an accuracy ranging from 0.518 to 0.800 (r = 0.715 ± 0.052; **Fig. 2e**) across HCP-YA participants and ranging from 0.475 to 0.775 (r = 0.684 ± 0.047; **Fig. 2f**) across HCP-D participants. The lowest individual-level structure-function coupling from GNN was higher than the highest coupling from the linear association in both datasets. Moreover, our individualized prediction accuracy from GNN was higher than that from fully-connected deep neural network as reported in prior work (i.e., r = 0.55 ± 0.1)[15]. Overall, these results indicated that the GNN framework detected the structure-function coupling better than both a linear association and a traditional fully-connected neural network.

We further explored how the network topology contributed to structure-function coupling. To do this, we rewired the SC to randomize the network topology but keep the distribution of nodal degree and strength[50]. Using the linear association, we found that the coupling between FC and rewired SC was r = 0.014 ± 0.006 (**Fig. 2e**) for HCP-YA participants and r = 0.018 ± 0.007 (**Fig. 2f**) for HCP-D participants. To evaluate how the network topology contributed to GNN-based structure-function coupling, we trained a GNN model with rewired SC using training data to predict the FC in the testing data. Similarly, we found GNN trained by rewired SC could only predict FC with an accuracy of r = 0.262 ± 0.045 (**Fig. 2e**) for individual participants in HCP-YA and r = 0.268 ± 0.038 (**Fig. 2f**) in HCP-D. Numerically, rewiring SC reduced the structure-function coupling by 64% (i.e., empirical: mean r = 0.715, rewired: mean r = 0.259) on average in HCP-YA, and by 61% (i.e., empirical: mean r = 0.684, rewired: mean r = 0.267) in HCP-D. As an alternative method to directly compare with one previous study[15], we kept the original SC in the training dataset to train the GNN model but rewired the SC in the testing set. As a result, the prediction performance was r = 0.080 ± 0.060 for testing participants in HCP-YA and r = 0.024 ±

0.012 in HCP-D. Therefore, rewiring SC in the testing set reduced the structure-function coupling by 89% (i.e., empirical: mean $r = 0.715$, rewired: mean $r = 0.080$) on average in HCP-YA, and by 96% (i.e., empirical: mean $r = 0.684$, rewired: mean $r = 0.024$) in HCP-D. In contrast, the study using fully-connected neural network reported that rewiring SC in the testing set reduced the coupling by 20% to 50%[15]. This comparison indicated that our GNN captured more higher-order network topological information in the coupling compared to the traditional fully-connected neural network. Overall, these results suggested that network topology drives the structure-function coupling.

After demonstrating the topological-driven structure-function coupling at the global (whole-brain) level, we next evaluated structure-function coupling at the regional level for both linear and GNN models. Specifically, we defined the structural profile of each cortical region as its connected SC edges for the linear model and its connected predicted FC edges for the GNN model. The functional profile for each cortical region was defined as all connected actual FC edges. Regional structure-function coupling was measured as the Pearson correlation between structural and functional profiles for each cortical region. We found that the regional structure-function coupling ranged from 0.086 to 0.587 for HCP-YA (**Fig. 2g**) and ranged from 0.070 to 0.654 for HCP-D (**Fig. 2h**) across all 400 cortical regions for the linear model. Using the GNN model, the regional structure-function coupling substantially increased, ranging from 0.316 to 0.829 for HCP-YA (**Fig. 2i**) and ranging from 0.287 to 0.817 for HCP-D (**Fig. 2j**) across the cortical regions. Importantly, for both linear and GNN models, regional structure-function coupling was heterogeneously distributed across the cortex, with a higher value in the primary sensorimotor cortices and a lower

value in the higher-order association cortices. This cortical pattern of structure-function coupling was consistent with prior literatures[10,11].

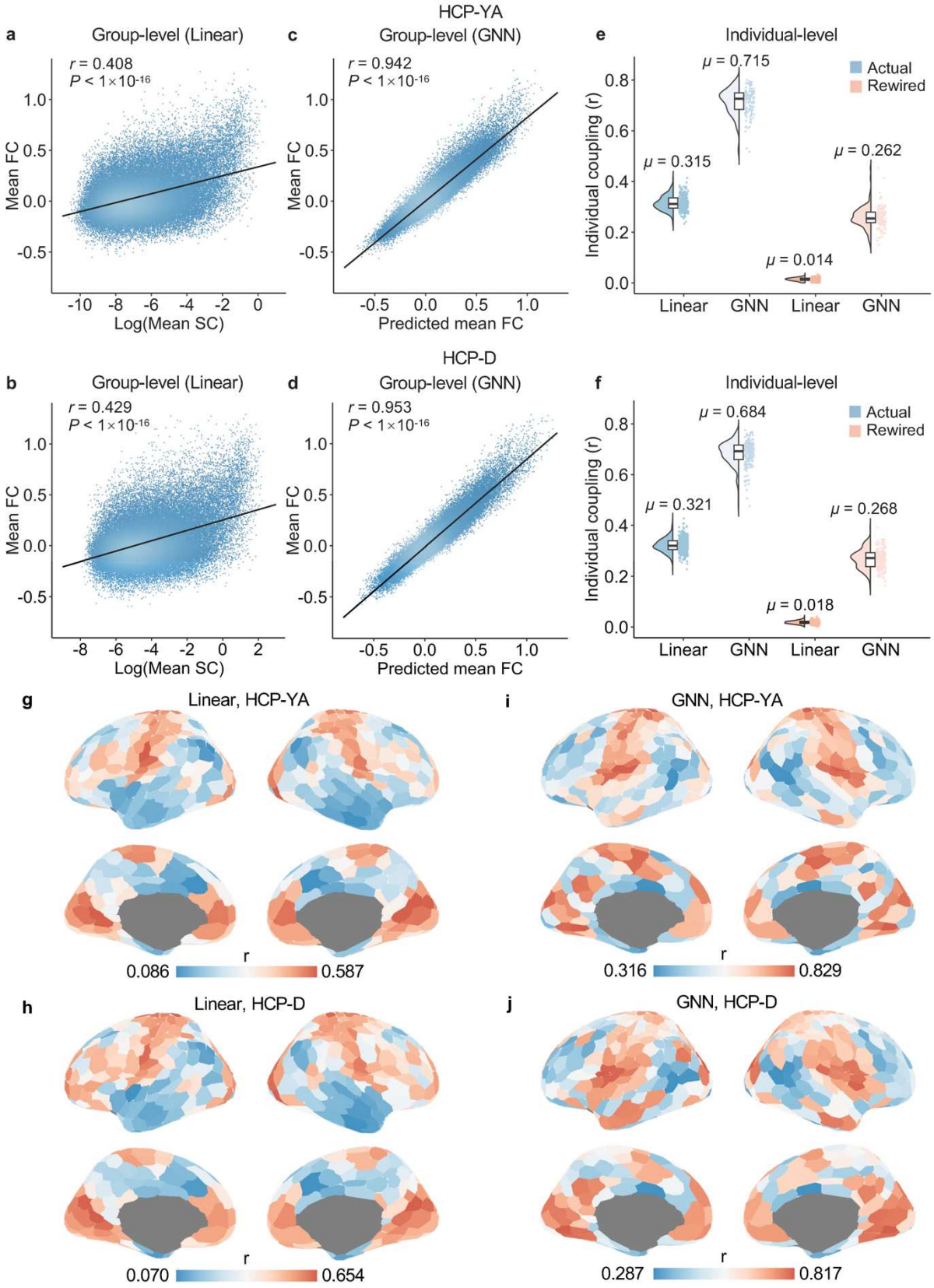

Fig. 2 | Structure-function coupling based on linear and GNN models. a,**b**, The group mean SC was significantly correlated with mean FC in the HCP-YA (**a**, $r = 0.408$, $P < 1\times10^{-16}$) and HCP-D (**b**, $r = 0.429$, $P < 1\times10^{-16}$) datasets, based on the linear Pearson correlation. **c**,**d**, GNN accurately predicted the group mean FC from the mean SC in both datasets. The predicted mean FC was significantly correlated with mean empirical FC in the HCP-YA (**c**, $r = 0.942$, $P < 1\times10^{-16}$) and HCP-D (**d**, $r = 0.953$, $P < 1\times10^{-16}$) datasets. **e**,**f**, At the individual participant level, GNN returned a much higher structure-function coupling than linear association in both HCP-YA (**e**, linear: $r = 0.315 \pm 0.029$; GNN: $r = 0.715 \pm 0.052$) and HCP-D (**f**, linear: $r = 0.321 \pm 0.027$; GNN: 0.684 ± 0.047) datasets. Moreover, rewiring the SC network by disrupting the network topology and keep the degree and strength distribution substantially reduced individuals' structure-function coupling from both linear and GNN models in both HCP-YA (**e**, linear: $r = 0.014 \pm 0.006$; GNN: $r = 0.262 \pm 0.045$) and HCP-D (**f**, linear: $r = 0.018 \pm 0.007$; GNN: 0.268 ± 0.038) datasets. This suggested the structure-function couplings were mainly driven by the network topology. **g**,**h**, The regional structure-function coupling by linear association for HCP-YA (**g**) and HCP-D (**h**) datasets. **i**,**j**, The regional structure-function coupling by the GNN model for HCP-YA (**i**) and HCP-D (**j**) datasets.

Structure-function coupling is primarily dominated by group-common effects, with subtle but significant individual effects

Having found that structure-function coupling was reliable and driven by network topology, we next examined the magnitudes of group-common and individual-specific effects in structure-function coupling, utilizing both linear and GNN models. To achieve this, we constructed a participant-by-participant matrix of structure-function coupling for both models. The diagonal elements of the matrix quantify the structure-function coupling within individuals, while the off-diagonal elements quantify the coupling between one participant's SC (or predicted FC when using GNN) and another participant's FC (**Fig. 3a**). We designated the within-individual coupling as 'matched coupling' and the between-individual coupling as 'mismatched coupling'.

As expected, we observed that the average of all pairs of matched coupling (Linear: HCP-YA: $r = 0.315$; HCP-D: $r = 0.321$; GNN: HCP-YA: $r = 0.715$; HCP-D: $r = 0.684$) was higher than the average of all pairs of mismatched coupling (Linear: HCP-YA: $r = 0.312$; HCP-D: $r = 0.318$; GNN:

HCP-YA: $r = 0.702$; HCP-D: $r = 0.666$) for both linear and GNN models. We defined the total effects of structure-function coupling as the average matched coupling, the group-common effects as the average mismatched coupling, and individual-specific effects as the difference between the average matched coupling and the average mismatched coupling. A similar approach has been used to evaluate the group and individual effects in functional networks[31]. Our results revealed that using the linear model, the individual effects accounted for 1.18% of the total effects of structure-function coupling in HCP-YA and 0.94% in HCP-D (**Fig. 3b**). In contrast, with the GNN model, the individual effects accounted for 1.74% of total effects in HCP-YA and 2.65% in HCP-D (**Fig. 3c**). These results indicated that GNN outperformed the linear association in capturing individual effects, suggesting some individual effects of structure-function coupling were explained by the non-linear high-order network topology. Moreover, both models demonstrated that structure-function coupling was primarily dominated by group-common factors (more than 97%) rather than individual-specific traits (less than 3%).

As the individual effects of structure-function coupling were minor for both models, we next evaluated whether the individual effects were statistically significant. To test this, we extracted the matched coupling and the average of all mismatched coupling for each participant (**Fig. 3d**). We compared the matched coupling and the average mismatched coupling across all participants statistically using two-tailed paired t-tests. The results indicated that the matched coupling was significantly higher than the mismatched coupling in both the linear model (HCP-YA: $P < 0.001$; HCP-D: $P < 0.0001$; **Fig. 3e**) and the GNN model (HCP-YA: $P < 0.0001$; HCP-D: $P < 0.0001$; **Fig. 3f**). These findings confirmed that the individual effects of structure-function coupling were statistically significant, as demonstrated in two independent datasets and two distinct approaches.

Overall, our findings suggested that individual structure-function coupling primarily reflected the group-common characteristics, with subtle yet significant individual-specific effects.

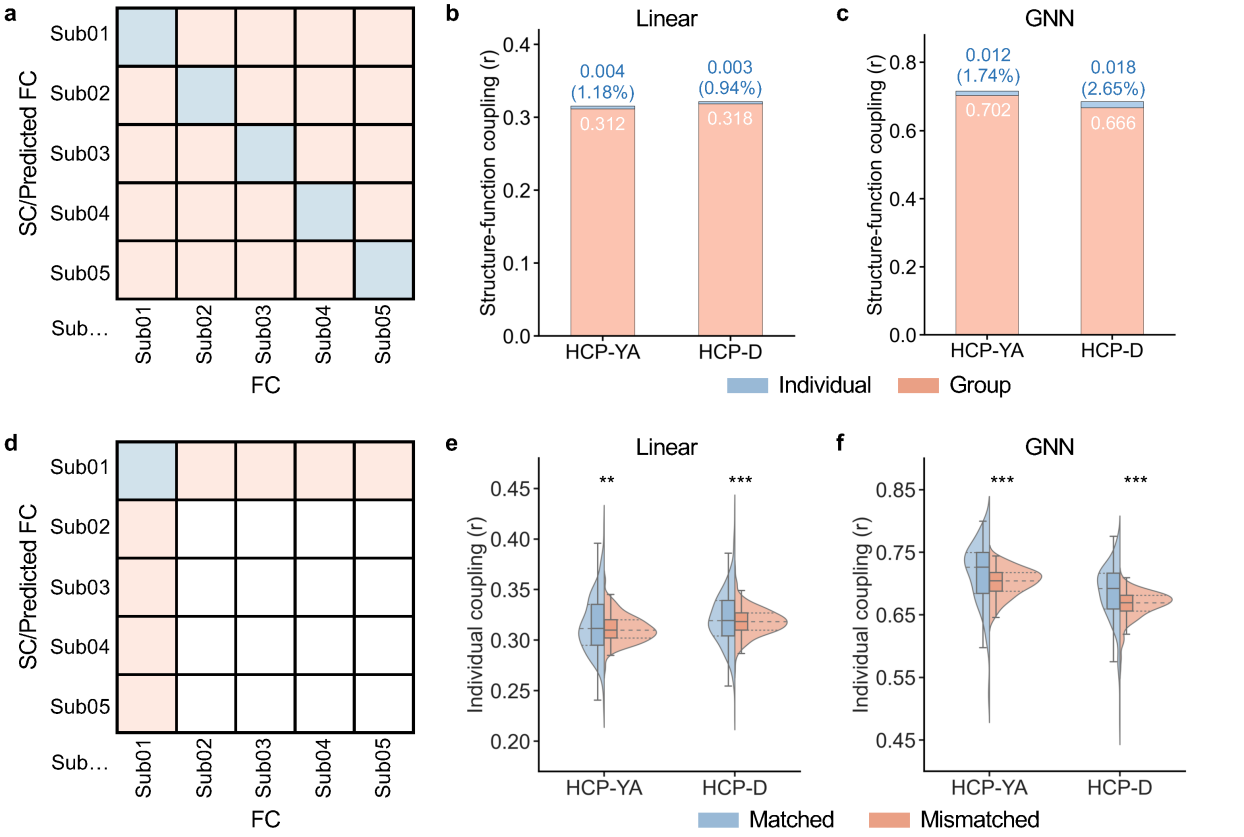

Fig. 3 | The group-common and individual-specific effects of structure-function coupling. a, The matrix of structure-function coupling between each pair of participants. Diagonal elements (cold color) represent the within-subject coupling (i.e., matched coupling), while off-diagonal elements (warm color) represent the coupling between one participant's SC or Predicted FC and another participant's FC (i.e., mismatched coupling). SC was used for the linear model and the predicted FC was used for GNN model to calculate the structure-function coupling. The total effects were defined as the average value of the diagonal elements; the group-common effects were defined as the average value of the off-diagonal elements; and the individual-specific effects were defined as their difference. **b**,**c**, The group and individual effects were estimated using the linear model (**b**, HCP-YA: 0.312/0.004; HCP-D: 0.318/0.003) and the GNN model (**c**, HCP-YA: 0.702/0.012; HCP-D: 0.666/0.018). **d**, The matched coupling and the average of all mismatched coupling were extracted for each participant and then were statistically compared across participants using two-tailed paired t-tests. **e**, **f**, The matched individual coupling was significantly higher than the mismatched coupling for both the linear model (**e**) and the GNN model (**f**),

suggesting statistically significant individual-specific effects of structure-function coupling. ** indicates $P < 0.001$, *** indicates $P < 0.0001$, two-tailed paired t-test.

Group and individual effects of structure-function coupling organize on the cortex along the sensorimotor-association axis

Having identified the magnitudes of group-common and individual-specific effects in structure-function coupling at the global level, we evaluated how group and individual effects were distributed across the cortex at the regional level. Recent studies have consistently demonstrated the sensorimotor-association cortical axis to be a unifying organizing principle of both anatomical and functional properties across cortex[25]. We hypothesized that the cortical distributions of both group and individual effects would align with the sensorimotor-association cortical axis. We acquired the priori cortical map of sensorimotor-association cortex axis (**Fig.4a**), which was derived by averaging diverse cortical neurobiological properties[25]. The cortical regions were continuously ranked along this axis, with the primary sensorimotor cortices representing the lowest ranks and the higher-order association cortices representing the highest ranks.

We next calculated the group and individual effects of GNN-based structure-function coupling at the regional level. We constructed a participant-by-participant matrix of GNN-based coupling and averaged all mismatched couplings for each cortical region, resulting in the regional group effects. We observed that the group effects were higher in the primary sensorimotor cortices and lower in the higher-order association cortices in both HCP-YA (**Fig.4b**) and HCP-D (**Fig.4c**) datasets. Using a Spearman rank correlation and a conservative spin-based spatial permutation test[51], we found that the cortical distributions of regional group effects were highly reproducible between the two datasets (Spearman's rho = 0.87, $P_{spin} < 0.001$). Using the linear model to evaluate the regional

structure-function coupling, we observed that the cortical distribution of group effects was similar to that using the GNN model in both HCP-YA and HCP-D datasets (**Fig.S2a**).

We next quantitatively evaluated whether the group effects of regional structure-function coupling were organized along the principal sensorimotor-association cortical axis. Using the Spearman correlation, we found that the group effects based on the GNN model were negatively correlated with the ranks of sensorimotor-association axis across all cortical regions in both HCP-YA (Spearman's rho = -0.48, $P_{spin} < 0.001$; **Fig. 4d**) and HCP-D (Spearman's rho = -0.32, $P_{spin} = 0.003$; **Fig. 4e**) datasets. The sensorimotor pole of the cortical axis showed a higher group effect, and the association pole showed a lower group effect. Additionally, using the linear model to evaluate structure-function coupling, we consistently observed a negative association between regional group effects and sensorimotor-association axis ranks in both HCP-YA (spearman's rho = -0.53, $P_{spin} < 0.001$; **Fig. S2b**) and HCP-D (Spearman's rho = -0.51, $P_{spin} = 0.001$; **Fig. S2c**). These results suggested that the sensorimotor-association cortical axis could potentially constrain the cortical distribution of group effects of structure-function coupling.

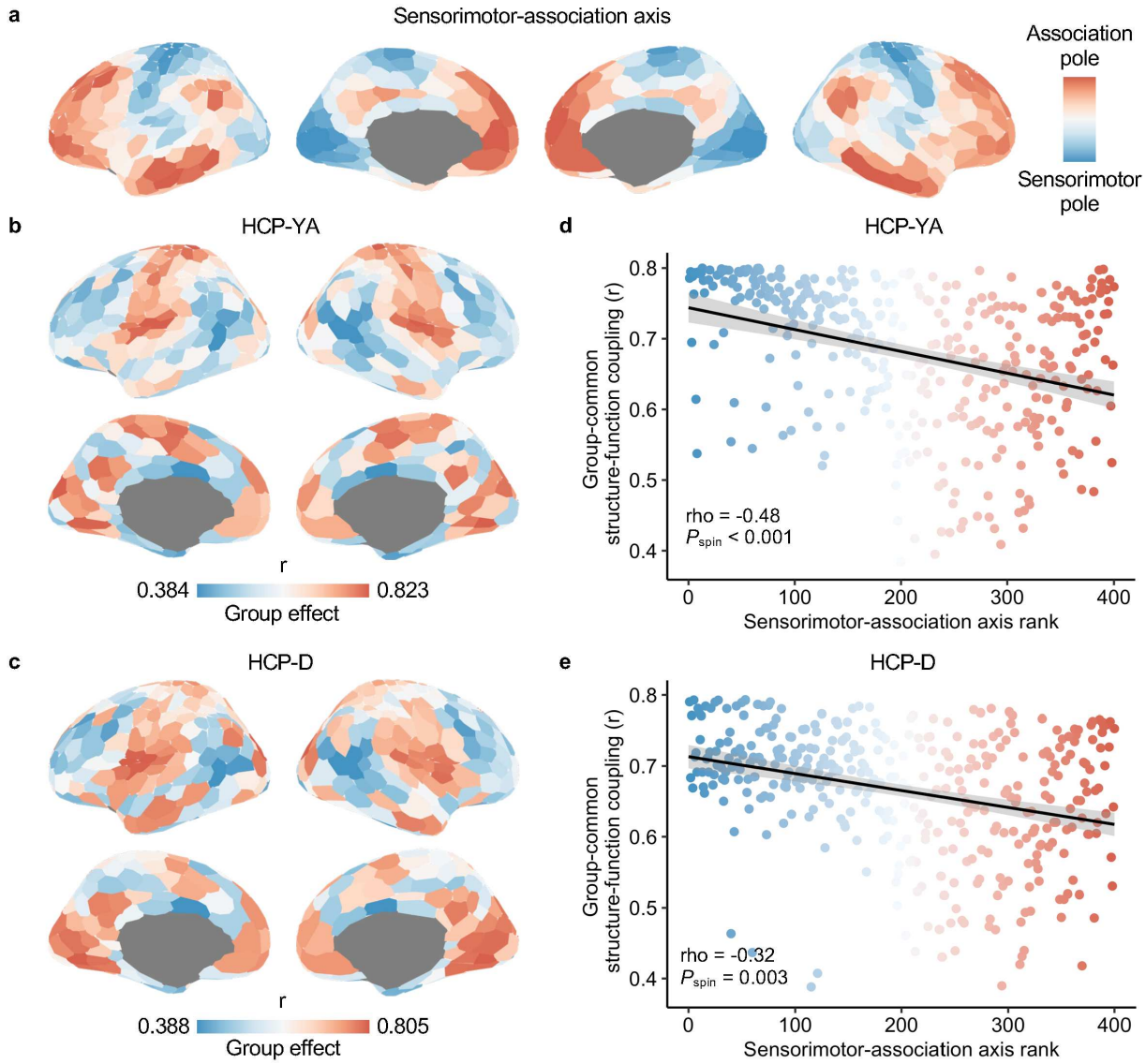

Fig. 4 | GNN-derived regional group-common structure-function effects inversely align with the sensorimotor-association cortical axis. a, The cortical map of the priori sensorimotor-association axis was derived from Sydnor et al.[25], where warm color represents association cortices with higher ranks and cold color represents sensorimotor cortices with lower ranks. **b**,**c**, The cortical map of group-common effects in regional structure-function coupling estimated by the GNN model in the HCP-YA (**b**) and HCP-D (**c**) datasets. **d**,**e**, The regional group effects of structure-function coupling were negatively correlated with the sensorimotor-association axis ranks in the HCP-YA (**d**, Spearman's rho = -0.48, $P_{spin} < 0.001$) and HCP-D (**e**, Spearman's rho = -0.32, $P_{spin} = 0.003$) datasets. The outliers (mean ± 3×SD) were excluded in the correlation analysis. Each point in the scatter plot represents a cortical region and is colored by its rank in sensorimotor-association axis.

We next examined the cortical distribution of the individual-specific effects of regional structure-function coupling. With regional participant-by-participant matrices of GNN-based structure-function coupling, we calculated individual effects as the difference between the average matched coupling and the average mismatched coupling for each cortical region. We observed that the individual-specific effects were lower in sensorimotor cortices and higher in association cortices in both the HCP-YA (**Fig. 5a**) and HCP-D (**Fig. 5b**) datasets. This cortical distribution of individual effects was significantly aligned between the two datasets (Spearman's rho = 0.33, P_{spin} < 0.001). Using the linear model, we observed a similar cortical pattern of individual effects as that with the GNN model in both datasets (**Fig.S2d**).

By quantifying the alignment with the sensorimotor-association cortical axis, we found a significantly positive correlation between the individual effects and the ranks of this cortical axis in both HCP-YA (Spearman's rho = 0.30, P_{spin} < 0.001; **Fig. 5c**) and HCP-D (Spearman's rho = 0.18, P_{spin} = 0.045; **Fig. 5d**) datasets. These results indicated an opposite cortical pattern in individual-specific effects compared to that of group-common effects. The sensorimotor pole of the axis had a lower individual effect of structure-function coupling, and the association pole showed a higher individual effect. However, using the linear model, the association between regional individual effects and cortical axis rank was not significant in either HCP-YA (Spearman's rho = 0.01, P_{spin} = 0.436; **Fig. S2e**) or HCP-D (Spearman's rho = -0.11, P_{spin} = 0.227; **Fig. S2f**) datasets. These results suggested that the GNN model is better at capturing the biologically meaningful individual-specific effects of structure-function coupling in the human brain.

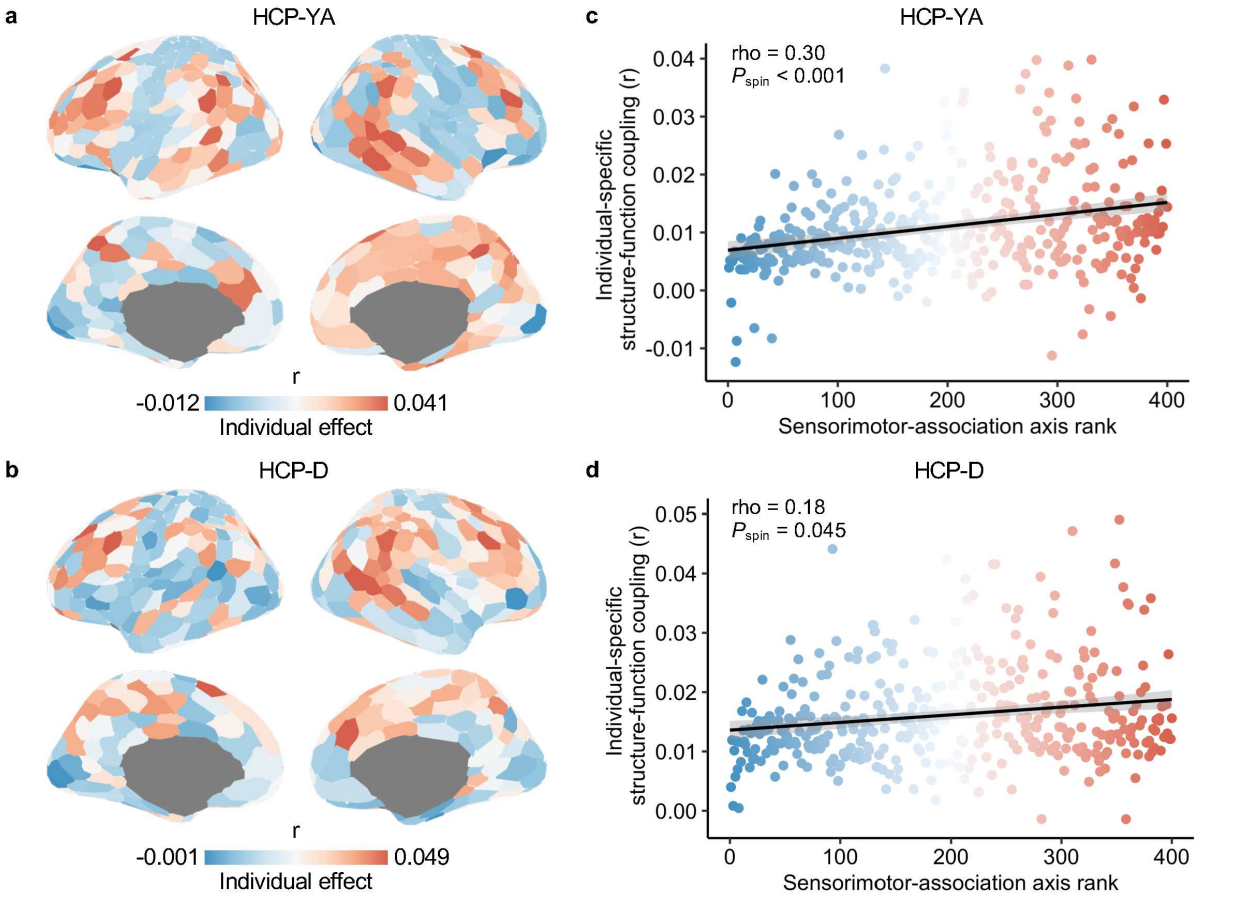

Fig. 5 | GNN-derived regional individual-specific effects of structure-function positively align with the sensorimotor-association cortical axis. a,**b**, The cortical map of individual-specific effects in structure-function coupling estimated by the GNN model in the HCP-YA (**a**) and HCP-D (**b**) datasets. **c**,**d**, The individual-specific effects were positively correlated with the ranks in the sensorimotor-association axis across all cortical regions in the HCP-YA (**c**, Spearman's rho = 0.30, P_{spin} < 0.001) and HCP-D (**d**, Spearman's rho = 0.18, P_{spin} = 0.045) datasets. The outliers (mean ± 3×SD) were excluded from the correlation analysis. Each point in the scatter plot represents a cortical region and is colored by its cortical axis rank.

Sensitivity analyses

We performed two additional analyses to ensure that our results were robust to the methodological choices. In this study, we defined the individual effects of the structure-function coupling by subtracting the average mismatched coupling (i.e., between-subject coupling) from the matched coupling (i.e., within-subject coupling). This measurement might be influenced by the magnitude of the total effects, as larger total effects can potentially generate larger individual effects. To

mitigate the potential scaling issue, we defined the normalized individual effects as the proportion of the individual effect to the total effect, and re-evaluated the alignment between the normalized individual effects and the sensorimotor-association cortical axis ranks. Similar to our main results, we found that the normalized individual effects were lower in sensorimotor cortices and higher in association cortices (Fig. **S3a** & **S3b**). Moreover, we obtained a significant positive correlation between individual effects and cortical axis ranks in the HCP-YA (Spearman's rho = 0.34, P_{spin} < 0.001; **Fig. S3c**) dataset and the HCP-D (Spearman's rho = 0.22, P_{spin} = 0.015; **Fig. S3d**) dataset.

We also tested how robust our result is with respect to the brain parcellation. In the main analyses, we constructed the structural and functional connectivity with Schaefer-400 atlas[43]. Here, we validated our GNN model in another Schaefer-200 parcellation. We first confirmed the significance of individual-specific structure-function coupling effects. We observed significant individual effects of the coupling with Schaefer-200 (**Fig. S4a**). Furthermore, we demonstrated the negative association between group effects and sensorimotor-association cortical axis ranks (**Fig. S4 b-d**) and the positive association between individual effects and cortical ranks (**Fig.S4 e-g**) across all regions. Overall, our main results were robust to the choice of cortical parcellations.

Discussion

In this study, we proposed a GNN framework to evaluate the magnitude of the group-common and individual-specific effects of structure-function coupling. We found that structural connectivity accurately predicted unseen individuals' functional connectivity with the GNN model, and this prediction was driven by network topology. We observed that structure-function coupling was dominated by the group-common characteristics, simultaneously, the minor individual-specific effects were also significant. Finally, we found that the regional group and individual effects both

hierarchically patterned across the cortex along the fundamental sensorimotor-association cortical axis. The sensorimotor pole of the axis showed a higher group effect and a lower individual effect, while the association pole showed a higher individual effect and a lower group effect of the structure-function coupling. These results were consistent between two independent, high-quality datasets. Our findings emphasized the importance of considering group and individual effects in both theoretical research of structure-function coupling and connectivity-based clinical therapeutics.

Understanding the dynamical communication process on the connectome of structural connectivity is a central goal of neuroscience[5,6]. Prior studies demonstrated that the structural connectivity of macroscale white matter tracts is associated with the functional connectivity measured by the correlation between pairs of regional time series[9-24]. The cortical distribution of the regional structure-function coupling aligns with the axis of the fundamental sensorimotor-association cortical hierarchy[10,11,25]. Moreover, the structure-function coupling changes with age and is related to individual differences in cognition and psychopathology[10,13,22,26,27]. Building on these studies, our work provided a systematic examination of the group-common and individual-specific effects of the structure-function coupling at the global and regional levels using both the linear association and the advanced GNN.

We found that, using the GNN framework, structural connectivity reconstructed with diffusion MRI accurately predicted unseen individuals' functional connectivity from resting-state fMRI. Consistent with our results, previous studies have consistently demonstrated a robust coupling between structure and functional connectivity using a variety of interpretable models, such as

linear associations[9-12], biophysical models[14], communication models[6,13,21,23,52], and the network control theory[53-56]. However, these interpretable models typically returned relatively small structure-function coupling values even when accounting for indirect communication, suggesting potentially imperfect alignment between structural and functional connectivity[6,7,24]. Recently, Sarwar and colleagues found that a fully-connected neural network predicted functional connectivity with much higher accuracy than interpretable models[15], suggesting the structure-function coupling could be higher than previously imagined. Two recent studies employed GNN to investigate structure-function coupling, however, they did not evaluate how the network topology contributed to the coupling[36,37]. Our results extended these findings by demonstrating that the GNN achieved higher structure-function coupling than fully-connected neural networks and this improvement was primarily contributed by network topology. Specifically, by randomizing the network topology of SC, our GNN model reduced the prediction accuracy by more than 89%, whereas the fully-connected neural network reduced 20%~50% as shown in this prior work[15]. This result demonstrated that the prediction using GNN was mainly driven by the network topology. Our result was also consistent with prior findings that GNN is better at capturing topological representations of network data, such as cellular networks[34] and protein networks[35], compared to traditional deep learning approaches.

Our results also demonstrated that the structure-function coupling was dominated by the group-common effects, and the remaining minor individual effects were also significant. The robust group effects could underlie the past success in the estimation of structure-function coupling at the group level[9,11,14,16,18-20]. This result was also consistent with prior studies showing that the functional networks were largely determined by group-common organizational principle[31] while

structural networks were even less variable than functional networks[32]. As a direct support for our results, one recent study also observed that the structure-function coupling based on a linear association was dominated by group effects, which were consistent across six datasets with different acquisitions or processing methods[32]. However, they found that the individual effects of structure-function coupling were only observed in one of the six datasets[32]. Here, using an advanced GNN approach and two independent, high-quality datasets, we demonstrated that the individual effects of structure-function coupling were also robust and reproducible. Moreover, our results indicated that the individual effects with the GNN approach were much larger than those with the linear association approach, which potentially explained non-stable individual effects in prior study with linear approach[32]. Future studies are warranted to examine how to improve interpretable network communication models to better detect the individual effects of structure-function coupling.

The sensorimotor-association cortical hierarchy has been proposed to be a unifying cortical organizing principle for diverse neurobiological properties, including structure, function, metabolic, transcription, and evolution[10,11,19,25,57-62]. Particularly, recent studies have demonstrated that the cortical distribution of structure-function coupling also aligns with the sensorimotor-association axis[10,11]. Consistent with these prior accounts, we found that both the group and individual effects of the regional structure-function coupling were hierarchically distributed across the cortex along the sensorimotor-association cortical axis. More specifically, we observed that the higher-order association cortex, which sits at the top end of the cortical axis, displayed the highest individual effects and the lowest group effects, while the primary sensorimotor cortex displayed the highest group effects and the lowest individual effects. Both structural and functional

connectivity exhibited the highest inter-individual variability in the association cortex and the lowest in the sensorimotor cortex[38,39], which could partly support our findings. Moreover, the sensorimotor cortex primarily comprises circuits with relatively simple and canonical feedforward and feedback connectivity patterns[63], which could potentially resulted in a high cross-individual similarity of structure-function coupling. In contrast, the association cortex exhibits a noncanonical circuit architecture with complicated and distributed connections[64], which could lead to individual diversity in the structure-function coupling.

Several potential limitations should be noted. First, precisely reconstructing individuals' white matter structural connectivity is challenging owing to the inherent limitations of diffusion MRI-based fiber tractography. In this study, we used a currently state-of-the-art probabilistic fiber tractography with multi-shell, multi-tissue constrained spherical deconvolution[44] and applied the anatomically constrained tractography[45] and spherical deconvolution informed filtering of tractograms[46] to improve the biological accuracy. Moreover, we used a consistency-based thresholding to reduce the influence of false positive connections[10]. Second, the current study did not analyze the structure-function coupling of subcortical and cerebellar structures, as these regions require specialized analysis procedures that are different from those applied to the cortex. Future studies may evaluate the group and individual effects of structure-function coupling in the subcortical and cerebellar regions. Finally, while the graph neural network accurately predicted functional connectivity with structural network topology, its black-box nature prevents us from understanding the underlying communication mechanism supporting the prediction. However, this result still provides a benchmark to optimize the interpretable models to explicitly explain how the structural connectome supports the functional connectivity.

Notwithstanding these limitations, we demonstrated that GNN captured a stronger topology-driven coupling between structural and functional connectivity than previous models, suggesting an avenue to improve current coupling models. Our results indicated that the individual effects of structure-function coupling were the highest in the association cortex, which was related to prolonged development of higher-order cognitions and confers to diverse psychopathologies[25]. This result implied that structure-function coupling could be a potential neuromarker to track individual differences in cognitive development and vulnerability to mental disorders. As structural connectivity pathway facilitated the propagation of neurostimulation-induced activity[21,65], our findings could have implications in clinical practice of neurostimulation. The dominated group effects in structure-function coupling could explain the experience that the same neurostimulation target (i.e., dorsal lateral pre-frontal cortex) has benefited many different patients[66]. Simultaneously, the significant individual-specific effects could explain that the personalized stimulation targets have improved the intervention effects for certain patients[67].

Methods

HCP young adult (HCP-YA) dataset

We acquired multi-modal neuroimaging data from 339 unrelated participants (156 males, aged 22–37) from the HCP young adult (HCP-YA) dataset (release S900), including T1-weighted structural, resting-state functional MRI (fMRI) and diffusion MRI[41]. All imaging data were acquired by a multiband sequence on a Siemens 3T Skyra scanner. Two resting-state fMRI sessions, with two runs in each session (left-right and right-left phase-encoding), were acquired for each participant with a resolution of 3 mm isotropic. Each resting-state run comprised 1,200

frames for approximately 15 min in length. For diffusion MRI, data were acquired in two runs with opposite phase-encoding directions for each participant. Each run included 270 non-collinear directions with 3 non-zero shells (b = 1000, 2000, and 3000 s/mm^2). Other details regarding the HCP-YA dataset and MRI acquisition parameters have been described in prior study[41].

HCP development dataset (HCP-D)

This study also comprised 633 participants (294 males, aged 8–21) obtained from the HCP-development (HCP-D) dataset (Release 2.0)[42]. All data were collected using a multiband EPI sequence on a 3T Siemens Prisma scanner. Two resting-state fMRI sessions were acquired for each participant, with two runs in each session, using anterior-posterior (AP) and posterior-anterior (PA) phase-encoding, respectively. Each resting-state run was approximately 6.5 min with 488 frames. Diffusion MRI data included two sessions, each with two non-zero shells (b = 1500, 3000 s/mm^2) and 185 diffusion-weighted directions. Further details about the HCP-D dataset have been described in previous study[42].

Structural and functional MRI data processing

Minimally preprocessed T1-weighted structural and functional MRI data were acquired from the HCP-D and HCP-YA datasets[68]. Briefly, structural MRI data were corrected for intensity non-uniformity, skull-stripped, and then used for cortical surface reconstruction. Volume-based structural images were segmented into cerebrospinal fluid (CSF), white matter, and gray matter, and spatially normalized to the standard MNI space. Functional MRI data were preprocessed with slice-timing, motion and distortion correction, co-registration to structural data, normalization to

MNI space, and projection to cortical surface. Functional timeseries were resampled to FreeSurfer's fsaverage space, and grayordinates files containing 91k samples were generated.

We then followed the post-processed protocols of eXtensible Connectivity Pipelines (XCP-D; https://xcp-d.readthedocs.io/en/latest/)[69]. Volumes with framewise-displacement (FD) greater than 0.3 were flagged as outliers and excluded[70-72]. We regressed out 36 nuisance regressors from the BOLD time series, including six motion parameters, global signal, mean white matter signal, and mean CSF signal, along with their temporal derivatives, quadratic terms, and quadratic derivatives[73]. Residual timeseries were then band-pass filtered (0.01–0.08 Hz) and spatially smoothed with a kernel size of FWHM = 6 mm. We further reduced the potential effects of head motion by excluding subjects with two criteria[74]. First, we dropped those fMRI runs that included more than 25% of the frames with FD > 0.2 mm. Second, we calculated the mean FD distribution for each fMRI run by pooling frames of all participants. Then, we derived the third quartile (Q3) and interquartile range (IQR) of this distribution. Runs with mean FD greater than 'Q3+1.5×IQR' were excluded. We excluded 218 HCP-D and 91 HCP-YA participants based on these two criteria. Additionally, three participants from the HCP-YA were excluded because of incomplete resting-state fMRI runs (less than 1,200 frames). Consequently, 415 participants (179 males, aged 8–21) from the HCP-D and 245 participants (114 males, aged 22–35) from the HCP-YA datasets were included in subsequent analyses.

Functional connectivity construction with functional MRI

Functional connectivity (FC) refers to the temporal correlation of functional MRI signals. For HCP-YA and HCP-D datasets, we constructed FC by the following procedures. First, we extracted

regional BOLD timeseries based on the a priori Schaefer parcellation with 400 parcels[43]. Next, FC was calculated as the Pearson correlation coefficient between each pair of regional BOLD timeseries, resulting in a 400×400 symmetrical FC matrix for each participant. We then applied Fisher's z-transformation to each FC value in the matrix. Finally, the 400 parcels were mapped onto the seven intrinsic networks from Yeo atlas[48], including the visual network (VIS), somatomotor network (SMN), dorsal attention network (DAN), ventral attention network (VAN), frontoparietal network (FPN), limbic network (LIM), and default mode network (DMN).

Diffusion MRI data processing

We used minimally preprocessed diffusion MRI data from the HCP-YA dataset[41]. The minimal preprocessing pipeline comprises b0 image intensity normalization across runs, EPI distortion correction, eddy current and motion correction, gradient nonlinearity correction, and registration to the native structural space (1.25 mm). The processed diffusion MRI data were further corrected for B1 field inhomogeneity using MRtrix3. Diffusion MRI data from HCP-D were preprocessed by QSIPrep (https://qsiprep.readthedocs.io/), an integrative platform for preprocessing and reconstructing diffusion MRI data[75], including tools from MRtrix3 (https://www.mrtrix.org/)[76]. Prior to preprocessing, we concatenated the two AP runs and the two PA runs, respectively, and selected the frames with b-value < 100 s/mm^2 as the b0 image. Next, we applied MP-PCA denoising, Gibbs unringing, and B1 field inhomogeneity correction through MRtrix3's *dwidenoise*[77], *mrdegibbs*[78], and *dwibiascorrect*[79] functions. FSL's eddy was then used for head motion correction and Eddy current correction[80]. Finally, the preprocessed DWI timeseries was resampled to ACPC space at a resolution of 1.5 mm isotropic. Particularly, a total of 11 participants from the HCP-D were excluded from subsequent structural connectivity analyses due to

incomplete DWI data (5 participants), tissue segmentation failure (5 participants), or the identification of isolated regions after tractography (1 participant). Therefore, a total of 245 participants from HCP-YA and 404 participants from HCP-D were analyzed in subsequent structure-function coupling analyses.

White matter structural network construction with diffusion MRI

We reconstructed whole-brain whiter matter tracts from preprocessed diffusion MRI data to construct the structural connectivity (SC). Reconstruction was conducted by the *mrtrix_multishell_msmt_ACT-hsvs* method in MRtrix3[76], which implements a multi-shell and multi-tissue constrained spherical deconvolution (CSD) to estimate the fiber orientation distribution (FOD) of each voxel[44]. Then, we followed the anatomically constrained tractography (ACT) framework to improve the biological accuracy of fiber reconstruction[45]. This tractography was performed by *tckgen*, which generates 40 million streamlines (length range from 30 to 250 mm, FOD power = 0.33) via a refined probabilistic streamlines tractography (iFOD2) based on the second-order integration over FOD. The streamlines were filtered from the tractogram based on the spherical deconvolution of the diffusion signal. We estimated the streamline weights using the command *tcksift2*[46]. Next, the SC matrix was constructed by *tck2connectome* based on the Schaefer-400 atlas for each participant. The edge weight of SC indicates the number of streamlines connecting two regions. For each connection, we normalized the edge weight by dividing the average volume of the corresponding two regions[81]. Furthermore, the edge weight of the SC matrix was log-transformed, which is commonly used to shift the non-Gaussian SC distribution to the Gaussian distribution in previous studies[7]. Finally, we obtained a 400×400 symmetric SC matrix for each participant. To address potential issues with spurious SC edges arising from probabilistic

tractography[82], we adopted a group-consistency thresholding approach as in previous studies[10,83]. We calculated the coefficient of variation (CV) for edge weight across participants and subsequently applied a threshold to individual structural connectivity matrices at the 75th percentile for edge weight CV. The top quartile of inconsistent connections were removed.

Predicting functional connectivity from structural connectivity using graph neural networks

The graph neural network (GNN) is a deep learning framework tailored for data of topological structure[84]. Different from other deep learning methodologies, such as fully-connected neural networks and convolutional neural networks, GNNs extract features based on the topological structure of the network. Since both SC and FC are topological data, a GNN can be used to investigate their topological relationship. To this end, we introduced a GNN framework to predict the empirical FC from SC and output the predicted FC. Our proposed GNN framework consists of two parts: (1) a two-layer graph convolutional network (GCN) to obtain node embeddings from the SC; (2) a two-layer multi-layer perceptron (MLP) that takes two node embeddings as inputs and predict the FC between them (**Fig.1a**).

Graph convolutional network. The main component of our graph neural network is the graph convolutional network (GCN)[47]. GCN generates node embeddings, representing the neighboring topological structure for each node. We denoted the node embedding generated from l^{th} layer GCN as $\boldsymbol{H}^l \in \mathbb{R}^{N \times C_l}$, where $l \in \{1, \dots, L\}$ represents the layer index and C_l represents the embedding dimension of layer l. H^0 is the exception representing the dimension of the input features of GCN. The input features are one-hot vectors that indicate the brain region of each node. Through message passing, the node embedding from the l^{th} layer will pass along the network connectivity, denoted

its adjacency matrix as $\boldsymbol{A}$, towards their neighboring nodes, convoluted by a GCN layer to get the node embedding of the $(l+1)^{\text{th}}$ layer. In our work, $\boldsymbol{A}$ is the adjacency matrix of SC, i.e., $\boldsymbol{A} \in \mathbb{R}^{K\times K}$. $K = 400$ is the number of nodes for the Schaefer-400 atlas. Therefore, the update equation of the node embedding from the l^{th} layer to the $(l+1)^{\text{th}}$ layer is denoted as:

$$\boldsymbol{H}^{l+1} = \mathrm{GCN}(\boldsymbol{H}^{l}, \boldsymbol{A})$$

With L layers in total, this message passing allows each node to embed its L-hop topological neighborhood. The concrete equation is formulated as:

$$\boldsymbol{H}^{l+1} = \mathrm{PReLU}(\widehat{\boldsymbol{D}}^{-\frac{1}{2}}\,\widehat{\boldsymbol{A}}\,\widehat{\boldsymbol{D}}^{\frac{1}{2}}\,\boldsymbol{H}^{l}\,\boldsymbol{W}^{l}_{\mathrm{GCN}})$$

where $\boldsymbol{W}^{l}_{\mathrm{GCN}} \in \mathbb{R}^{C_l\times C_{l+1}}$ is the trainable weight at the l^{th} layer. $\widehat{\boldsymbol{A}}$ is the adjacency matrix with self-loop added, i.e., $\widehat{\boldsymbol{A}} = \boldsymbol{A} + \boldsymbol{I}_K$, where $\boldsymbol{I}_K \in \mathbb{R}^{K\times K}$ is the K-dimension identity matrix. $\widehat{\boldsymbol{D}}$ is the diagonal matrix, with the diagonal value $\widehat{D}_{ii}$ equals to the nodal strength of node i in $\boldsymbol{A}$. As such, $\widehat{\boldsymbol{D}}^{-1/2}\,\widehat{\boldsymbol{A}}\,\widehat{\boldsymbol{D}}^{1/2}$ is the symmetric normalized Laplacian of the SC. We adopted the PReLU (Parametric Rectified Linear Unit) as the activation function due to its superior performance[85]:

$$\mathrm{PReLU}(x) = \begin{cases} x & x \geq 0 \\ \alpha x & x < 0\,,\ \alpha \text{ is trainable} \end{cases}$$

Multilayer perceptron. Subsequently, we used a pair of node embeddings as input to predict the functional connectivity between them by a two-layer multi-layer perceptron (MLP) with ReLU (Rectified Linear Unit) as the activation function (i.e., $\mathrm{ReLU}(x) = \max(0, x)$) after the first output layer. No activation function was used for the second layer. Specifically, for two node embeddings of node i and j, represented by $h_i, h_j \in H$, the predicted FC, termed $\mathrm{pFC}_{ij} \in \mathbf{pFC}$, between them is calculated as:

$$\mathrm{pFC}_{ij} = \mathrm{MLP}\left(h_i\,, h_j, \boldsymbol{W}_{\mathrm{MLP}}\right) \in \mathbf{pFC}$$

Model training and validation. To train our graph neural network model, we minimized the mean square error between the predicted FC and empirical FC with L2-regularizaion:

$$L_{\mathrm{MSE}} = \frac{1}{N_b} \sum_{n=1\ldots N_b} \frac{1}{M(M-1)} \sum_{i,j=1\ldots K;\, i\neq j} \left(\mathrm{pFC}_{ij} - \mathrm{eFC}_{ij}\right)^2 + \lambda \left|\boldsymbol{W}_{\mathrm{MLP}}\right|^2$$

where $\mathrm{eFC}_{ij} \in \mathbf{eFC}$ is the empirical FC between node i and j. We adopted L2-regularization on the MLP's weights with regularization parameter λ. We trained the model through batched gradient descent with a batch of N_b subjects and the Adam optimizer[86]. In addition, since FC is a symmetric matrix, we employed the $(\mathrm{pFC}_{ij} + \mathrm{pFC}_{ji})/2$ as the final predicted FC between node i and j for testing and further analysis. For both datasets, we randomly split 50% of the subjects as the training set, with the remaining 50% for testing and subsequent structure-function coupling analysis. By grid search based on the model's performance for 5-fold cross validation on the training set, we set the hyperparameter as: layer number (L=2), dimension for GCN (400×256×256), dimension for MLP (512×64×1), batch size (2), learning rate (0.0001), regularization parameter (λ=0.0001), and training epochs (400). The graph network model was built and trained using Pytorch and PyTorch Geometric. More details about implementations could be found in the code repository at https://github.com/PeiyuChen2023/GNN_SC_FC.

Structure-function coupling measured by linear and GNN models

In this work, we evaluated the structure-function coupling using both a linear model and our proposed GNN model. The linear model assesses the Pearson correlation between SC and FC, focusing solely on direct connections with nonzero edge strength. However, functional connectivity can emerge from polysynaptic communication on structural connectome[5,6]. The GNN

has the capability to capture both the direct and indirect functional communications based on the sparse SC. For each dataset, all participants were split into two subsets with one used as training and another used as testing set. The GNN model trained on all participants in the training set was used to predict the FC for the testing participants with their SC as input. The structure-function coupling was calculated as the Pearson correlation between the predicted and empirical FC for each participant in the testing set. At the group level, we used the model from training data and all testing participants' average SC as input to predict the average FC. We calculated the Pearson correlation between the predicted and empirical average FC as the structure-function coupling at the group level.

We also estimated the structure-function coupling at both the whole-brain and regional levels. At the whole-brain level, we extracted the upper triangle elements (79,800 unique edges) from either the 400×400 SC matrix or the predicted FC matrix, creating a structural profile vector. Simultaneously, we extracted the upper triangle elements from the empirical FC matrix, forming a functional profile vector. We calculated the Pearson correlation between the structural profile and functional profile across all connections at global level. At the regional level, we first defined the regional structural and functional profiles. For the i^{th} cortical region, we defined its structural or functional profile as the connections to all other cortical regions, which were represented by the i^{th} row (399×1) from the connection matrix. The regional structure-function coupling was determined by calculating the Pearson correlation between the structural profile and functional profile of each cortical region, enabling us to generate a cortical map of regional structure-function coupling for both the linear and GNN models. Notably, all participants were involved and analyzed

in the linear model based coupling, whereas the structure-function coupling based on the GNN model were derived from the testing set, comprising 50% of the participants.

Calculating group-common and individual-specific effects in structure-function coupling

A previous study indicated that the individual FC is contributed by both group-common and stable individual-specific factors[31]. Following the similar approach, we aimed to distinguish between group-common and individual-specific effects in structure-function coupling using both linear and GNN models. To achieve this, we computed the structure-function coupling both within-individual and between each pair of different participants, resulting in a participant-by-participant asymmetrical matrix of structure-function coupling (**Fig. 3a**). In this matrix, the element in the i^{th} row (SC or predicted FC from subject *i*) and j^{th} column (FC from subject *j*), termed as $\text{cp}_{i,j}$, represents the structure-function coupling between the i^{th} and j^{th} participants. The diagonal elements of the matrix measure the structure-function coupling within individual, while the off-diagonal elements estimate the coupling between one individual's SC and another individual's FC. We referred to the within-individual coupling and between-individual coupling as 'matched coupling' and 'mismatched coupling', respectively. In this study, we treated the averaged between-individual coupling as a group-common variance in the coupling across populations. This strategy has been used in prior study of effects in function networks[31]. We supposed that the total effects of within-individual coupling encompass both group-common and individual-specific effects. Therefore, we defined the group-common and individual-specific effects of structure-function coupling as follows:

$$\text{cp}_{\text{group}} = \frac{1}{N(N-1)} \sum_{i,j=1\ldots N;\ i\neq j} \text{cp}_{i,j}$$

$$\mathrm{cp}_{\mathrm{individual}} = \frac{1}{N}\sum_{i=1\ldots N} \mathrm{cp}_{i,i} - \mathrm{cp}_{\mathrm{group}}$$

where N corresponds to the number of participants. Given our finding that individual structure-function coupling is primarily dominated by the group-common effect, with minor individual-specific effects (see **Results**), we proceeded to assess the statistical significance of these individual effects. For this purpose, we defined the matched coupling and mismatched coupling for each subject (**Fig. 3d**). Specifically, the mismatched coupling of subject i was defined by the averaged coupling from all elements in the i^{th} row (SC or predicted FC from subject i, FC from other subjects) and i^{th} column (FC from subject i, SC or predicted FC from other subjects), except the within-individual coupling. The matched and mismatched coupling for each subject i is defined as:

$$\mathrm{cp}_{\mathrm{match},i} = \mathrm{cp}_{i,i}$$

$$\mathrm{cp}_{\mathrm{mismatch},i} = \frac{1}{2(N-1)}\sum_{j=1\ldots N;\ j\neq i} \left(\mathrm{cp}_{i,j} + \mathrm{cp}_{j,i}\right)$$

We considered the individual-specific coupling effects significant if matched coupling were statistically higher than mismatched coupling across participants. We conducted a two-sided paired t-test to examine the differences between matched coupling and mismatched coupling across all participants.

These analyses of group and individual effects in the coupling were first performed at the global level and then applied to each cortical region. It is noteworthy that only nonzero edges were examined in the linear model for both whole-brain and regional analyses.

Alignment between cortical maps of group and individual effects of structure-function coupling and the sensorimotor-association cortical axis

The sensorimotor-association axis has been consistently reported as a unifying organizing principle of both anatomical and functional properties across cortex[25]. A previous study has also identified a negative association between structure-function coupling and sensorimotor-association axis rank[10]. Here, we further investigated how group-common and individual-specific coupling align with the sensorimotor-association cortical axis, respectively. We acquired a cortical map of sensorimotor-association axis parcellated with Schaefer-400 atlas from Sydnor et al.[25]. Cortical regions were continuously ranked along this axis, with the primary sensorimotor cortices representing the lowest ranks and the higher-order association cortices representing the highest ranks. For both linear and GNN models, we calculated the Spearman' rank correlation to assess the alignment between the sensorimotor-association cortical axis and regional group-common effects as well as individual-specific effects across all cortical regions.

Null models

Rewiring networks. To evaluate the contribution of network topology in structure-function coupling, we utilized the Maslov-Sneppen rewiring algorithm to rewire individual SC. This process retained fundamental topological properties such as nodal degree and strength while randomizing topological structure. Furthermore, rewired networks preserved inter-node communication without creating isolated nodes. This algorithm was implemented via the Python version of the Brain Connectivity Toolbox (https://github.com/aestrivex/bctpy)[87]. For the linear model, we rewired SC from all individuals and re-evaluated the Pearson correlation between the rewired SC and FC for each participant. For the GNN model, we employed two strategies to assess

the impact of network topology. Firstly, we aimed to evaluate how much the GNN model could learn from the higher-order topology, so we only rewired SC in training data to acquire a topological-null GNN model. We did not rewire the SC in the testing set. We next used this topological-null GNN model to predict FC from SC in the testing set. Then, we re-evaluated the Pearson correlation between the predicted FC and FC for each participant in the testing set. Secondly, we trained the GNN model with the original SC and utilized the rewired SC to predict FC in the testing set. We again re-evaluated the Pearson correlation between the predicted FC and FC for each participant in the testing set. This strategy aimed to directly compare the contribution of the SC topology to our GNN with its contribution to the fully-connected network in a prior study[15].

Spin test. We employed the spin test to evaluate the significance of the spatial correspondence between group-common and individual-specific effects of structure-function coupling and sensorimotor-association cortical axis[51]. Particularly, the spin test generated a null distribution by randomly rotating brain maps while maintaining the original spatial covariance structure[51]. This approach projected the group and individual effects onto a spherical cortical surface of the FreeSurfer's fsaverage space and then randomly rotated 10,000 times to generate a list of rotated maps. Next, we calculated the Spearman's rank correlation between each rotated map and the sensorimotor-association axis map to construct a null distribution. The P value (P_{spin}) was determined by calculating the ratio of instances whose null correlations exceeded the empirical correlation coefficients.

Sensitivity analyses

One main result of this study is that the individual-specific effects of structure-function coupling showed a hierarchical pattern across the cortex that positively aligned with the sensorimotor-association cortical axis. However, as individual-specific effects are derived by subtracting the group-common effects from total effects of the coupling, larger total effects might numerically lead to larger individual-specific effects. To address this potential scaling issue, we defined the 'normalized individual effect' by dividing the individual effect by the total regional structure-function coupling, representing the proportion of the individual effect to the total effect. Subsequently, we reevaluated the alignment between the normalized individual effects and the ranks of the sensorimotor-association cortical axis for the GNN model.

We also assessed the robustness of our main results to another cortical parcellations. In addition to the Schaefer atlas comprising 400 cortical regions used in our primary analyses, we validated our GNN models using the Schaefer atlas with 200 cortical regions[43]. First, we constructed the connectome of FC and SC for each participants using the Shcaefer-200 and retrained the GNN model. Then, we distinguished the group-common and individual-specific effects of structure-function coupling, and verified the significance of individual-specific effects with Schaefer-200. Finally, we obtained the cortical maps of group-common and individual-specific effects of structure-function coupling and re-evaluated their alignment with the sensorimotor-association cortical axis. Specifically, leveraging the vertex-wise surface map of sensorimotor-association axis in the fsLR-32k space[25], we computed the parcel-level sensorimotor-association axis rank values of Schaefer-200 by averaging rank values from all vertices within each parcel.

Data availability

The HCP-YA and HCP-D datasets are available at https://db.humanconnectome.org/.

Code availability

All code used to perform the analyses in this study can be found at https://github.com/PeiyuChen2023/GNN_SC_FC.

Acknowledgements

This work is supported by the STI 2030-Major Projects (2022ZD0211300), Beijing Nova Program (Z211100002121002), and CIBR funds. Data were provided [in part] by the Human Connectome Project, WU-Minn Consortium (Principal Investigators: David Van Essen and Kamil Ugurbil; 1U54MH091657) funded by the 16 NIH Institutes and Centers that support the NIH Blueprint for Neuroscience Research; and by the McDonnell Center for Systems Neuroscience at Washington University. The HCP-Development 2.0 Release data used in this report came from DOI: 10.15154/1520708. Research reported in this publication was supported by the National Institute of Mental Health of the National Institutes of Health under Award Number U01MH109589 and by funds provided by the McDonnell Center for Systems Neuroscience at Washington University in St. Louis.

Author contributions

Z.C. and P.C. designed the study. P.C. and H.Y. performed the analyses with support from T.S.O. H.Y. and X.X. completed data preprocessing. X.Z., H.J. and J.H. replicated the model training and testing. H.Y and P.C. created the figures. Z.C. and T.S.O. supervised the project. R.C. provided resources. P.C., H.Y., and Z.C. wrote the manuscript with review and editing from all other authors.

Competing interests

The authors declare no competing interests.

References

1 Sporns, O. The human connectome: a complex network. *Annals of the New York Academy of Sciences* **1224**, 109-125 (2011). https://doi.org:10.1111/j.1749-6632.2010.05888.x

2 Bassett, D. S. & Bullmore, E. Small-world brain networks. *The Neuroscientist : a review journal bringing neurobiology, neurology and psychiatry* **12**, 512-523 (2006). https://doi.org:10.1177/1073858406293182

3 Sporns, O. & Betzel, R. F. Modular Brain Networks. *Annu Rev Psychol* **67**, 613-640 (2016). https://doi.org:10.1146/annurev-psych-122414-033634

4 van den Heuvel, M. P. & Sporns, O. Network hubs in the human brain. *Trends in cognitive sciences* **17**, 683-696 (2013). https://doi.org:10.1016/j.tics.2013.09.012

5 Avena-Koenigsberger, A., Misic, B. & Sporns, O. Communication dynamics in complex brain networks. *Nat Rev Neurosci.* **19**, 17-33 (2017). https://doi.org:10.1038/nrn.2017.149

6 Seguin, C., Sporns, O. & Zalesky, A. Brain network communication: concepts, models and applications. *Nat Rev Neurosci* (2023). https://doi.org:10.1038/s41583-023-00718-5

7 Suárez, L. E., Markello, R. D., Betzel, R. F. & Misic, B. Linking Structure and Function in Macroscale Brain Networks. *Trends in cognitive sciences* **24**, 302–315 (2020). https://doi.org:10.1016/j.tics.2020.01.008

8 Lynn, C. W. & Bassett, D. S. The physics of brain network structure, function and control. *Nature Reviews Physics* **1**, 318-332 (2019). https://doi.org:10.1038/s42254-019-0040-8

9 Honey, C. J. *et al.* Predicting human resting-state functional connectivity from structural connectivity. *Proceedings of the National Academy of Sciences of the United States of America* **106**, 2035-2040 (2009). https://doi.org:10.1073/pnas.0811168106

10 Baum, G. L. *et al.* Development of structure-function coupling in human brain networks during youth. *Proceedings of the National Academy of Sciences of the United States of America* **117**, 771-778 (2020). https://doi.org:10.1073/pnas.1912034117

11 Vazquez-Rodriguez, B. *et al.* Gradients of structure-function tethering across neocortex. *Proceedings of the National Academy of Sciences of the United States of America* **116**, 21219-21227 (2019). https://doi.org:10.1073/pnas.1903403116

12 Gu, Z., Jamison, K. W., Sabuncu, M. R. & Kuceyeski, A. Heritability and interindividual variability of regional structure-function coupling. *Nat Commun* **12**, 4894 (2021). https://doi.org:10.1038/s41467-021-25184-4

13 Zamani Esfahlani, F., Faskowitz, J., Slack, J., Misic, B. & Betzel, R. F. Local structure-function relationships in human brain networks across the lifespan. *Nat Commun* **13**, 2053 (2022). https://doi.org:10.1038/s41467-022-29770-y

14 Deco, G. *et al.* Resting-state functional connectivity emerges from structurally and dynamically shaped slow linear fluctuations. *J Neurosci* **33**, 11239-11252 (2013). https://doi.org:10.1523/JNEUROSCI.1091-13.2013

15 Sarwar, T., Tian, Y., Yeo, B. T. T., Ramamohanarao, K. & Zalesky, A. Structure-function coupling in the human connectome: A machine learning approach. *Neuroimage* **226**, 117609 (2021). https://doi.org:10.1016/j.neuroimage.2020.117609

16 Misic, B. *et al.* Network-Level Structure-Function Relationships in Human Neocortex. *Cereb Cortex* **26**, 3285-3296 (2016). https://doi.org:10.1093/cercor/bhw089

17 Hermundstad, A. M. *et al.* Structural foundations of resting-state and task-based functional connectivity in the human brain. *Proceedings of the National Academy of Sciences of the*

United States of America **110**, 6169-6174 (2013). https://doi.org:10.1073/pnas.1219562110

18 Suárez, L. E., Richards, B. A., Lajoie, G. & Misic, B. Learning function from structure in neuromorphic networks. *Nature Machine Intelligence* **3**, 771-786 (2021).

19 Demirtas, M. *et al.* Hierarchical Heterogeneity across Human Cortex Shapes Large-Scale Neural Dynamics. *Neuron* **101**, 1181-1194 e1113 (2019). https://doi.org:10.1016/j.neuron.2019.01.017

20 Misic, B. *et al.* Cooperative and Competitive Spreading Dynamics on the Human Connectome. *Neuron* **86**, 1518-1529 (2015). https://doi.org:10.1016/j.neuron.2015.05.035

21 Seguin, C. *et al.* Communication dynamics in the human connectome shape the cortex-wide propagation of direct electrical stimulation. *Neuron* **111**, 1391-1401 e1395 (2023). https://doi.org:10.1016/j.neuron.2023.01.027

22 Medaglia, J. D. *et al.* Functional Alignment with Anatomical Networks is Associated with Cognitive Flexibility. *Nat Hum Behav* **2**, 156-164 (2018). https://doi.org:10.1038/s41562-017-0260-9

23 Betzel, R. F. *et al.* Structural, geometric and genetic factors predict interregional brain connectivity patterns probed by electrocorticography. *Nat Biomed Eng* **3**, 902-916 (2019). https://doi.org:10.1038/s41551-019-0404-5

24 Valk, S. L. *et al.* Genetic and phylogenetic uncoupling of structure and function in human transmodal cortex. *Nat Commun* **13**, 2341 (2022). https://doi.org:10.1038/s41467-022-29886-1

25 Sydnor, V. J. *et al.* Neurodevelopment of the association cortices: Patterns, mechanisms, and implications for psychopathology. *Neuron* **109**, 2820-2846 (2021). https://doi.org:10.1016/j.neuron.2021.06.016

26 Jiang, X. *et al.* Connectome analysis of functional and structural hemispheric brain networks in major depressive disorder. *Transl Psychiatry* **9**, 136 (2019). https://doi.org:10.1038/s41398-019-0467-9

27 Jiang, H. *et al.* Structural-functional decoupling predicts suicide attempts in bipolar disorder patients with a current major depressive episode. *Neuropsychopharmacology* **45**, 1735-1742 (2020). https://doi.org:10.1038/s41386-020-0753-5

28 Soman, S. M. *et al.* Cortical structural and functional coupling during development and implications for attention deficit hyperactivity disorder. *Transl Psychiatry* **13**, 252 (2023). https://doi.org:10.1038/s41398-023-02546-8

29 Zarkali, A. *et al.* Organisational and neuromodulatory underpinnings of structural-functional connectivity decoupling in patients with Parkinson's disease. *Commun Biol* **4**, 86 (2021). https://doi.org:10.1038/s42003-020-01622-9

30 Cocchi, L. *et al.* Disruption of structure-function coupling in the schizophrenia connectome. *Neuroimage Clin* **4**, 779-787 (2014). https://doi.org:10.1016/j.nicl.2014.05.004

31 Gratton, C. *et al.* Functional Brain Networks Are Dominated by Stable Group and Individual Factors, Not Cognitive or Daily Variation. *Neuron* **98**, 439-452 e435 (2018). https://doi.org:10.1016/j.neuron.2018.03.035

32 Zimmermann, J., Griffiths, J., Schirner, M., Ritter, P. & McIntosh, A. R. Subject specificity of the correlation between large-scale structural and functional connectivity. *Netw Neurosci* **3**, 90-106 (2019). https://doi.org:10.1162/netn_a_00055

33 Zhou, J. *et al.* Graph neural networks: A review of methods and applications. *AI Open* **1**, 57-81 (2020). https://doi.org:10.1016/j.aiopen.2021.01.001

34 Wu, Z. *et al.* Graph deep learning for the characterization of tumour microenvironments from spatial protein profiles in tissue specimens. *Nat Biomed Eng* **6**, 1435-1448 (2022). https://doi.org:10.1038/s41551-022-00951-w

35 Gao, Z. *et al.* Hierarchical graph learning for protein-protein interaction. *Nat Commun* **14**, 1093 (2023). https://doi.org:10.1038/s41467-023-36736-1

36 Neudorf, J., Kress, S. & Borowsky, R. Structure can predict function in the human brain: a graph neural network deep learning model of functional connectivity and centrality based on structural connectivity. *Brain Structure and Function* **227**, 331-343 (2022). https://doi.org:10.1007/s00429-021-02403-8

37 Hong, Y. *et al.* Structural and functional connectome relationships in early childhood. *Developmental Cognitive Neuroscience* **64**, 101314 (2023). https://doi.org:10.1016/j.dcn.2023.101314

38 Mueller, S. *et al.* Individual variability in functional connectivity architecture of the human brain. *Neuron* **77**, 586-595 (2013). https://doi.org:10.1016/j.neuron.2012.12.028

39 Huang, W. *et al.* Individual Variability in the Structural Connectivity Architecture of the Human Brain. *bioRxiv*, 2023.2001. 2011.523683 (2023). https://doi.org:10.1101/2023.01.11.523683

40 Buckner, R. L. & Krienen, F. M. The evolution of distributed association networks in the human brain. *Trends in cognitive sciences* **17**, 648-665 (2013). https://doi.org:10.1016/j.tics.2013.09.017

41 Van Essen, D. C. *et al.* The WU-Minn Human Connectome Project: An overview. *NeuroImage* **80**, 62-79 (2013). https://doi.org:10.1016/j.neuroimage.2013.05.041

42 Somerville, L. H. *et al.* The Lifespan Human Connectome Project in Development: A large-scale study of brain connectivity development in 5-21 year olds. *NeuroImage* **183**, 456-468 (2018). https://doi.org:10.1016/j.neuroimage.2018.08.050

43 Schaefer, A. *et al.* Local-Global Parcellation of the Human Cerebral Cortex from Intrinsic Functional Connectivity MRI. *Cerebral Cortex* **28**, 3095-3114 (2018). https://doi.org:10.1093/cercor/bhx179

44 Jeurissen, B., Tournier, J.-D., Dhollander, T., Connelly, A. & Sijbers, J. Multi-tissue constrained spherical deconvolution for improved analysis of multi-shell diffusion MRI data. *NeuroImage* **103**, 411-426 (2014). https://doi.org:10.1016/j.neuroimage.2014.07.061

45 Smith, R. E., Tournier, J.-D., Calamante, F. & Connelly, A. Anatomically-constrained tractography: improved diffusion MRI streamlines tractography through effective use of anatomical information. *NeuroImage* **62**, 1924-1938 (2012). https://doi.org:10.1016/j.neuroimage.2012.06.005

46 Smith, R. E., Tournier, J.-D., Calamante, F. & Connelly, A. SIFT2: Enabling dense quantitative assessment of brain white matter connectivity using streamlines tractography. *NeuroImage* **119**, 338-351 (2015). https://doi.org:10.1016/j.neuroimage.2015.06.092

47 Kipf, T. N. & Welling, M. Semi-Supervised Classification with Graph Convolutional Networks. (2017). https://doi.org:10.48550/arXiv.1609.02907

48 Thomas Yeo, B. T. *et al.* The organization of the human cerebral cortex estimated by intrinsic functional connectivity. *Journal of Neurophysiology* **106**, 1125-1165 (2011). https://doi.org:10.1152/jn.00338.2011

49 Rousselet, G. A., Pernet, C. R. & Wilcox, R. R. The percentile bootstrap: a primer with step-by-step instructions in R. *Advances in Methods and Practices in Psychological Science* **4**, 2515245920911881 (2021).

50 Vasa, F. & Misic, B. Null models in network neuroscience. *Nat Rev Neurosci* (2022). https://doi.org:10.1038/s41583-022-00601-9

51 Alexander-Bloch, A. F. *et al.* On testing for spatial correspondence between maps of human brain structure and function. *Neuroimage* **178**, 540-551 (2018). https://doi.org:10.1016/j.neuroimage.2018.05.070

52 Seguin, C., Mansour, L. S., Sporns, O., Zalesky, A. & Calamante, F. Network communication models narrow the gap between the modular organization of structural and functional brain networks. *Neuroimage* **257**, 119323 (2022). https://doi.org:10.1016/j.neuroimage.2022.119323

53 Gu, S. *et al.* Optimal trajectories of brain state transitions. *Neuroimage* **148**, 305-317 (2017). https://doi.org:10.1016/j.neuroimage.2017.01.003

54 Betzel, R. F., Gu, S., Medaglia, J. D., Pasqualetti, F. & Bassett, D. S. Optimally controlling the human connectome: the role of network topology. *Scientific reports* **6**, 30770 (2016). https://doi.org:10.1038/srep30770

55 Stiso, J. *et al.* White Matter Network Architecture Guides Direct Electrical Stimulation through Optimal State Transitions. *Cell Rep* **28**, 2554-2566 e2557 (2019). https://doi.org:10.1016/j.celrep.2019.08.008

56 Cui, Z. *et al.* Optimization of energy state transition trajectory supports the development of executive function during youth. *eLife* **9** (2020). https://doi.org:10.7554/eLife.53060

57 Burt, J. B. *et al.* Hierarchy of transcriptomic specialization across human cortex captured by structural neuroimaging topography. *Nat Neurosci* **21**, 1251-1259 (2018). https://doi.org:10.1038/s41593-018-0195-0

58 Margulies, D. S. *et al.* Situating the default-mode network along a principal gradient of macroscale cortical organization. *Proceedings of the National Academy of Sciences of the United States of America* **113**, 12574-12579 (2016). https://doi.org:10.1073/pnas.1608282113

59 Huntenburg, J. M., Bazin, P. L. & Margulies, D. S. Large-Scale Gradients in Human Cortical Organization. *Trends in cognitive sciences* **22**, 21-31 (2018). https://doi.org:10.1016/j.tics.2017.11.002

60 Murray, J. D. *et al.* A hierarchy of intrinsic timescales across primate cortex. *Nat Neurosci* **17**, 1661-1663 (2014). https://doi.org:10.1038/nn.3862

61 Raut, R. V., Snyder, A. Z. & Raichle, M. E. Hierarchical dynamics as a macroscopic organizing principle of the human brain. *Proceedings of the National Academy of Sciences of the United States of America* **117**, 20890-20897 (2020). https://doi.org:10.1073/pnas.2003383117

62 Hill, J. *et al.* Similar patterns of cortical expansion during human development and evolution. *Proceedings of the National Academy of Sciences of the United States of America* **107**, 13135-13140 (2010). https://doi.org:10.1073/pnas.1001229107

63 Felleman, D. J. & Van Essen, D. C. Distributed hierarchical processing in the primate cerebral cortex. *Cereb Cortex* **1**, 1-47 (1991). https://doi.org:10.1093/cercor/1.1.1-a

64 Goldman-Rakic, P. S. Topography of cognition: parallel distributed networks in primate association cortex. *Annu Rev Neurosci* **11**, 137-156 (1988). https://doi.org:10.1146/annurev.ne.11.030188.001033

65 Sydnor, V. J. *et al.* Cortical-subcortical structural connections support transcranial magnetic stimulation engagement of the amygdala. *Sci Adv* **8**, eabn5803 (2022). https://doi.org:10.1126/sciadv.abn5803

66 Hyde, J. *et al.* Efficacy of neurostimulation across mental disorders: systematic review and meta-analysis of 208 randomized controlled trials. *Mol Psychiatry* **27**, 2709-2719 (2022). https://doi.org:10.1038/s41380-022-01524-8

67 Klooster, D. C. W., Ferguson, M. A., Boon, P. & Baeken, C. Personalizing Repetitive Transcranial Magnetic Stimulation Parameters for Depression Treatment Using Multimodal Neuroimaging. *Biol Psychiatry Cogn Neurosci Neuroimaging* **7**, 536-545 (2022). https://doi.org:10.1016/j.bpsc.2021.11.004

68 Glasser, M. F. *et al.* The Minimal Preprocessing Pipelines for the Human Connectome Project. *NeuroImage* **80**, 105-124 (2013). https://doi.org:10.1016/j.neuroimage.2013.04.127

69 Ciric, R. *et al.* Mitigating head motion artifact in functional connectivity MRI. *Nature Protocols* **13**, 2801-2826 (2018). https://doi.org:10.1038/s41596-018-0065-y

70 Power, J. D. *et al.* Methods to detect, characterize, and remove motion artifact in resting state fMRI. *NeuroImage* **84**, 320-341 (2014). https://doi.org:10.1016/j.neuroimage.2013.08.048

71 Satterthwaite, T. D. *et al.* An improved framework for confound regression and filtering for control of motion artifact in the preprocessing of resting-state functional connectivity data. *NeuroImage* **64**, 240-256 (2013). https://doi.org:10.1016/j.neuroimage.2012.08.052

72 Satterthwaite, T. D. *et al.* Heterogeneous impact of motion on fundamental patterns of developmental changes in functional connectivity during youth. *NeuroImage* **83**, 45-57 (2013). https://doi.org:10.1016/j.neuroimage.2013.06.045

73 Ciric, R. *et al.* Benchmarking of participant-level confound regression strategies for the control of motion artifact in studies of functional connectivity. *NeuroImage* **154**, 174-187 (2017). https://doi.org:10.1016/j.neuroimage.2017.03.020

74 Faskowitz, J., Esfahlani, F. Z., Jo, Y., Sporns, O. & Betzel, R. F. Edge-centric functional network representations of human cerebral cortex reveal overlapping system-level architecture. *Nature Neuroscience* **23**, 1644-1654 (2020). https://doi.org:10.1038/s41593-020-00719-y

75 Cieslak, M. *et al.* QSIPrep: an integrative platform for preprocessing and reconstructing diffusion MRI data. *Nature Methods* **18**, 775-778 (2021). https://doi.org:10.1038/s41592-021-01185-5

76 Tournier, J.-D. *et al.* MRtrix3: A fast, flexible and open software framework for medical image processing and visualisation. *NeuroImage* **202**, 116137 (2019). https://doi.org:10.1016/j.neuroimage.2019.116137

77 Veraart, J. *et al.* Denoising of diffusion MRI using random matrix theory. *NeuroImage* **142**, 394-406 (2016). https://doi.org:10.1016/j.neuroimage.2016.08.016

78 Kellner, E., Dhital, B., Kiselev, V. G. & Reisert, M. Gibbs-ringing artifact removal based on local subvoxel-shifts. *Magnetic Resonance in Medicine* **76**, 1574-1581 (2016). https://doi.org:10.1002/mrm.26054

79 Tustison, N. J. *et al.* N4ITK: Improved N3 Bias Correction. *IEEE Transactions on Medical Imaging* **29**, 1310-1320 (2010). https://doi.org:10.1109/TMI.2010.2046908

80 Andersson, J. L. R., Graham, M. S., Zsoldos, E. & Sotiropoulos, S. N. Incorporating outlier detection and replacement into a non-parametric framework for movement and distortion correction of diffusion MR images. *NeuroImage* **141**, 556-572 (2016). https://doi.org:10.1016/j.neuroimage.2016.06.058

81 Hagmann, P. *et al.* Mapping the Structural Core of Human Cerebral Cortex. *PLOS Biology* **6**, e159 (2008). https://doi.org:10.1371/journal.pbio.0060159

82 Roberts, J. A., Perry, A., Roberts, G., Mitchell, P. B. & Breakspear, M. Consistency-based thresholding of the human connectome. *NeuroImage* **145**, 118-129 (2017). https://doi.org:10.1016/j.neuroimage.2016.09.053

83 Ge, J. *et al.* Increasing diversity in connectomics with the Chinese Human Connectome Project. *Nat Neurosci* **26**, 163-172 (2023). https://doi.org:10.1038/s41593-022-01215-1

84 Bessadok, A., Mahjoub, M. A. & Rekik, I. Graph Neural Networks in Network Neuroscience. *IEEE Transactions on Pattern Analysis and Machine Intelligence* **45**, 5833-5848 (2023). https://doi.org:10.1109/TPAMI.2022.3209686

85 You, J., Ying, R. & Leskovec, J. Design Space for Graph Neural Networks. (2021). https://doi.org:10.48550/arXiv.2011.08843

86 Kingma, D. P. & Ba, J. Adam: A Method for Stochastic Optimization. (2017). https://doi.org:10.48550/arXiv.1412.6980

87 Rubinov, M. & Sporns, O. Complex network measures of brain connectivity: Uses and interpretations. *NeuroImage* **52**, 1059-1069 (2010). https://doi.org:10.1016/j.neuroimage.2009.10.003